PAPER

Complex structures generated by competing interactions in harmonically confined colloidal suspensions

IOP Publishing Journal of Physics: Condensed Matter
J. Phys.: Condens. Matter **30** (2018) 325101 (8pp) https://doi.org/10.1088/1361-648X/aad14f

Complex structures generated by competing interactions in harmonically confined colloidal suspensions

E O Lima[1], P C N Pereira[1], H Löwen[2] and S W S Apolinario[1]

[1] Departamento de Física, Universidade Federal de Pernambuco, 50670-901 Recife, PE, Brazil
[2] Institut für Theoretische Physik II: Soft Matter, Heinrich-Heine-Universität, Düsseldorf, Universitätsstraße 1, 40225 Düsseldorf, Germany

E-mail: Hartmut.Loewen@uni-duesseldorf.de and sergiowsa@df.ufpe.br

Received 10 May 2018, revised 26 June 2018
Accepted for publication 5 July 2018
Published 23 July 2018

Abstract

We investigate the structural properties of colloidal particle systems interacting via an isotropic pair potential and confined by a three-dimensional harmonic potential. The interaction potential has a repulsive–attractive–repulsive profile that varies with the interparticle distance (also known as a 'mermaid' potential). We performed Langevin dynamics simulations to find the equilibrium configurations of the system. We show that particles can self-assemble in complex structural patterns, such as compact disks, fringed disks, rods, spherical clusters with superficial entrances among others. Also, for particular values of the parameters of the interaction potential, we could identify that some configurations were formed by quasi two-dimensional (2D) structures which are stable for 2D systems.

Keywords: self-assembly, colloidal suspensions, 'mermaid' potential

(Some figures may appear in colour only in the online journal)

1. Introduction

Colloidal suspensions of mesoscopic spherical particles are excellent classical model systems for fundamental questions of structural phase transformations [1–5]. The effective interactions between these particles can largely be tuned by charges and additives such that complex interactions with different competing length scales can be realized [6]. In the past two decades we have started to understand better how such interactions govern the stable ground state of the bulk system. For example, quasicrystals have been shown to evolve in one-component three-dimensional (3D) colloidal systems provided the interaction is complex enough [7, 8] and isostructural solid–solid transition were predicted [9–12]. In fact, various complex crystalline lattices have been found to be stable for certain parameters at small temperature [13–18].

One particular sort of interaction potential has been explored in great detail in the bulk. It is the so-called 'mermaid potential', a term coined by G Stell, which comprises potentials with an attractive head and a repulsive tail [19, 20]. This interaction is also known as short-ranged-attraction–long-ranged repulsion (SALR) potential and is realizable in principle in charged and magnetic colloidal suspensions and protein solutions with additives [20, 21]. A lot of theoretical work has been devoted to these 'mermaid potentials' [22]. In the 3D bulk, the competition between the two length scales of attraction and repulsion results in quite complex stable structures which are reminiscent to those obtained for amphihilic systems [23] and block-copolymers [24]. These include stable cluster fluids [21, 25–29], cluster solids and new mesomorphic structures [30] with hexagonal rod-like, lamellar [31–33] or gyroid [34, 35] topologies. Based on this recent work, at small temperatures, a general bulk phase topology was obtained with a stable lamellar phase at intermediate densities surrounded by a double gyroid phase and different stable cluster crystal phases (such as *hcp* and *bcc* lattices) and hexagonal ordered rod-structures hence a huge treasure of structures can be stable or metastable [35].

Colloidal suspensions can also be confined in external confining potential using e.g. optical tweezers, thermophoretic traps [36] and acoustic trapping devices [37]. The simplest description of such a trapping potential is a harmonic or isotropic parabolic potential. It is known from colloids and

complex plasmas [38–41] that the constraints posed by confinement generate new cluster structures which can be vastly different from the unconfined bulk system [42–45].

In this paper we combine the two aspects of competing SALR interactions and harmonic confinement. In this context, previous calculations have been performed in two spatial dimensions only [46–49]. They have revealed that complex two-dimensional (2D) structures emerge at zero temperature which incorporate the length scales involved in the pair interaction and therefore show a wealth of structures e.g. with fringed rims. Here we use the same model potential as previously applied to 2D and tackle the more-complicated 3D systems. Motivated from the rich bulk structures occurring in three dimensions, we expect even more complex structures which share at least parts of the bulk structures (gyroids, lamellar, etc). Indeed, we find a wealth of different structures which are so complex that they cannot even be classified easily. Some of them are reminiscent of the bulk building blocks, some can be seen as stacks of the structures found in the pure 2D system, and many others generated by the confinement are unfamiliar and new. In fact, for certain selected parameter combinations of our model, we show that at zero temperature cluster structures emerge which have superficial entrances, clusters which look like stacks of fringed disks, assemblies of parallel rods and compact aggregates with holes and tunnels. Some macroscopic patterns are correlated to a packing measure from which we construct a phase diagram.

Most of these cluster structures are novel, demonstrating the rich potential to construct cluster morphologies at will by using tailored pair interactions and confinement. These tailored clusters can be used as further building blocks for micron-sized sieves and filters of controlled porosity [50]. They can also be taken as complex aggregates to form self-organized crystals on larger length scales.

The paper is organized as follows: in section 2, we propose the model and describe our simulation technique and protocol. Results are summarized in section 3 and we conclude in section 4.

2. Theoretical model and simulation

We study the cooling scenario of a 3D system composed of N monodisperse colloids confined in a parabolic potential. The inter-particle interaction potential is given by

$$U(r_{ij}) = U^{HC}(r_{ij}) + U^{PW}(r_{ij}) + U^{G}(r_{ij}), \tag{1}$$

where r_{ij} is the distance between the centers of the colloids i and j, $U^{HC}(r_{ij})$ denotes a short range soft-core potential, $U^{PW}(r_{ij})$ a mid-range well potential, and $U^{G}(r_{ij})$ a shifted Gaussian shaped potential acting at larger distances. The explicit expressions for these three parts of the potential are

$$U^{HC}(r_{ij}) = \varepsilon \left(\frac{D}{r_{ij}}\right)^{m}, \tag{2a}$$

$$U^{PW}(r_{ij}) = -\varepsilon \exp\left[-\left(\frac{r_{ij}-D}{\alpha}\right)^{l}\right], \tag{2b}$$

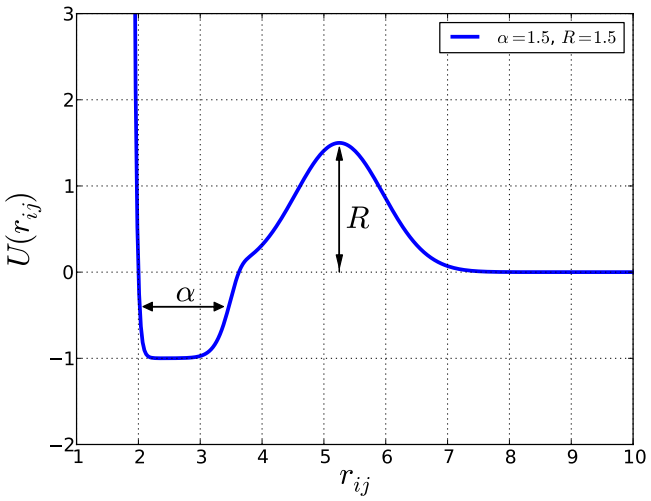

Figure 1. Representation of the interaction potential for the parameters $\alpha = 1.5$ and $R = 1.5$.

$$U^{G}(r_{ij}) = R\varepsilon \exp\left[-\left(\frac{r_{ij}-\beta}{0.5D}\right)^{2}\right], \tag{2c}$$

where D defines the diameter of the colloids, ε gives the strength of the short-ranged repulsion, m and l are exponents that define, respectively, the range of the left and right sides of the total potential well, α is an important parameter which defines the thickness of the well, while R and β are parameters used, respectively, to change the height of the Gaussian barrier and shift its position along the radial direction. In this work we use the value $\beta = 1.5(D+\alpha)$ in order to avoid superposition between the terms $U^{PW}(r_{ij})$ and $U^{G}(r_{ij})$. Henceforth we use $D/2$ (the radius) and ε as our length and energy scales, respectively. Figure 1 shows a graphic representation of the inter-particle interaction potential given by equation (1) for the particular situation of $\alpha = 1.5$ and $R = 1.5$. It clearly has a 'mermaid' structure with a short-ranged attraction and a longer-ranged repulsion and therefore belongs to the general class of SALR interactions.

The specific assumptions in modeling the attractive and repulsive parts are a bit special for our model potential. Our choice was motivated by the fact that the same model has been studied already in 2D previously. Moreover, almost any model potential can be realized experimentally in colloidal suspensions provided enough different interactions types (such as van der Waals, steric, screened Coulomb due to charging, depletion attraction or accumulation repulsion due to additives, dipole–dipole interactions) are superimposed.

The external confinement potential acting on the particle i is a parabolic one, which is given by the expression

$$V(r_i) = \frac{1}{2}\kappa r_i^2, \tag{3}$$

where the prefactor κ defines its strength and r_i is the particle i radial distance to the origin. Therefore, we can write the total potential energy of the system as

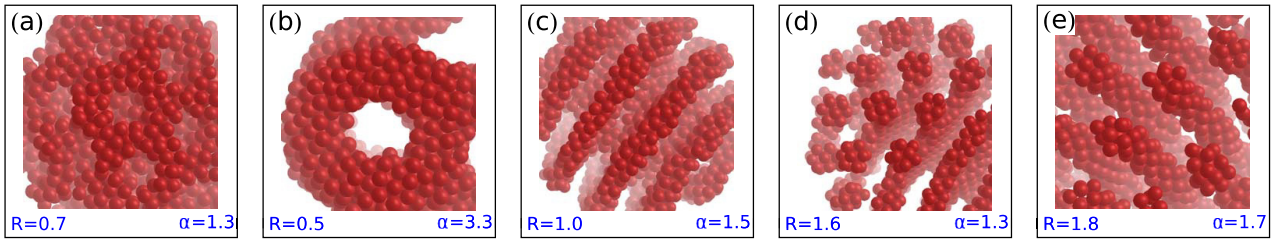

Figure 2. Examples of mesoscale patterns present in the structures: (a) spherical structure with superficial entrances, (b) tunneled structures, (c) parallel disk structures, (d) separated fringed disks and (e) parallel rods. The parameters R and α are indicated within the figures. Figures are enlarged images of the obtained clusters, whose viewing angles were chosen to highlight as best as possible the various patterns.

$$U_{\rm tot} = \sum_{i=1}^{N} V(r_i) + \sum_{i=1}^{N-1}\sum_{j>i}^{N} U(r_{ij}). \tag{4}$$

In order to obtain the self-assembled configurations of the system we use a simulated annealing scheme. For a certain set of parameters, the particles are arranged randomly in a cubic box of side $L = 50D$ centered at the origin, while the temperature of the system is set to the value $T_i = 5\varepsilon/k_{\rm B}$. In the sequence, the temperature is slowly decreased to $T_f = 0$. For a given temperature, the evolution of the system is given by the overdamped Langevin equation, that is integrated using Euler's method, and therefore resulting in the following first order algorithm

$$\vec{r}_i(t+\Delta t) = \vec{r}_i(t) + \frac{\vec{F}_i(t)\Delta t}{\gamma} + \vec{g}\sqrt{2k_{\rm B}T\Delta t}, \tag{5}$$

where $\vec{F}_i = -\nabla_{\vec{r}_i} U_{\rm tot}$ is the total force acting on particle i, Δt is the finite time step of the integrator and $\vec{g}$ is a 3D vector with random components, following a standard normal distribution whose mean and variance are equal to zero and one, respectively. The viscous drag coefficient is set to $\gamma = 1$ and the time scale is $t_0 = \gamma D^2/\varepsilon$.

A good convergence of the integration algorithm in equation (5) is achieved for $\Delta t = 10^{-5}$. For each temperature T, we iterated the system 5×10^4 time steps before decreasing the temperature by an amount of $\Delta T = 0.05$.

In our investigation we considered systems with $N = 1792$ particles. The number N is large enough to see an internal cluster structure but small enough to be treated numerically. Throughout our analysis, some potential parameters were fixed ($m = 50$, $l = 10$, $\varepsilon = 1$ and $\kappa = 0.1$), while we considered the parameters R and α within the range $\{0.1, 5.0\}$ with steps of 0.1.

Our main aim is to find the structures that can be self-assembled by annealing. This does not necessarily imply that we arrive at the true groundstate for long times as many metastable configuration can occur in principle for SALR potentials. However, when we started our simulation from different initial configurations, we arrived always at clusters which had the same global topology and the same mesoscopic structure (for the same values of R and α), although the particle positions were not identical.

3. Results and discussions

In order to outline the rich variety of macroscopic patterns, we present in figure 2 some examples. Only appropriate cutouts of the full cluster are shown here. In the case of figure 2(a), where $R = 0.7$ and $\alpha = 1.3$, the structure looks spherical with superficial entrances. When the attractive part of the interaction is broader (e.g. for $R = 0.5$ and $\alpha = 3.3$), tunnels are observed as seen in figure 2(b). For $R = 1.0$ and $\alpha = 1.5$, the configuration is formed by almost parallel disks which are connected near their centers (see figure 2(c)). Comparatively, for increasing R and decreasing α, e.g. for $R = 1.6$ and $\alpha = 1.3$, the parallel disks give place to non-connected disks having fringed borders, as demonstrated in figure 2(d). Finally, we found that particles can aggregate to form rods, as seen in figure 2(e) for $R = 1.8$ and $\alpha = 1.7$. This corresponds to the bulk hexagonal rod phase which is modified under harmonic confinement. Also, in figures 2(c)–(e), some preferential direction appears, thus breaking the isotropy of the confinement. This is expected given the fact that already in the bulk the isotropy is broken for the structured phases.

As already stated, the kind of potential considered in this paper was used in previous 2D simulations (see [47, 51]). The structures found in these previous works called our attention due to their peculiarity and variety. We notice that the 3D self-assembled structures, for some values of the interaction potential parameters, can be viewed as structures composed by quasi-2D sub-structures. These latter resemble the 2D equilibrium configurations found in [47, 51]. In this case some analogy can be drawn between 3D and 2D systems.

For instance, the tunneled structures found in this work (see, for instance, figure 2(b)), could be viewed as the 3D version of the 2D perforated clusters in [47]. To put it in a more operational way, the 3D structure with tunnels can be generated by a successive stacking of 2D structures corresponding to circular clusters with holes. Regardless of the dimensionality of the system, holes and tunnels are patterns that can decrease the total energy because they diminish the contribution given by the energy barrier of the Gaussian interaction potential.

Figure 2(c) can be perceived as a structure constructed by the stacking of few quasi-2D compact disks. The latter are analogous to the 2D compact disks shown, for instance, in figure 7(e1) of [47]. Of course, in this case, the comparison can not be taken literally, in the sense that, first, the compact discs

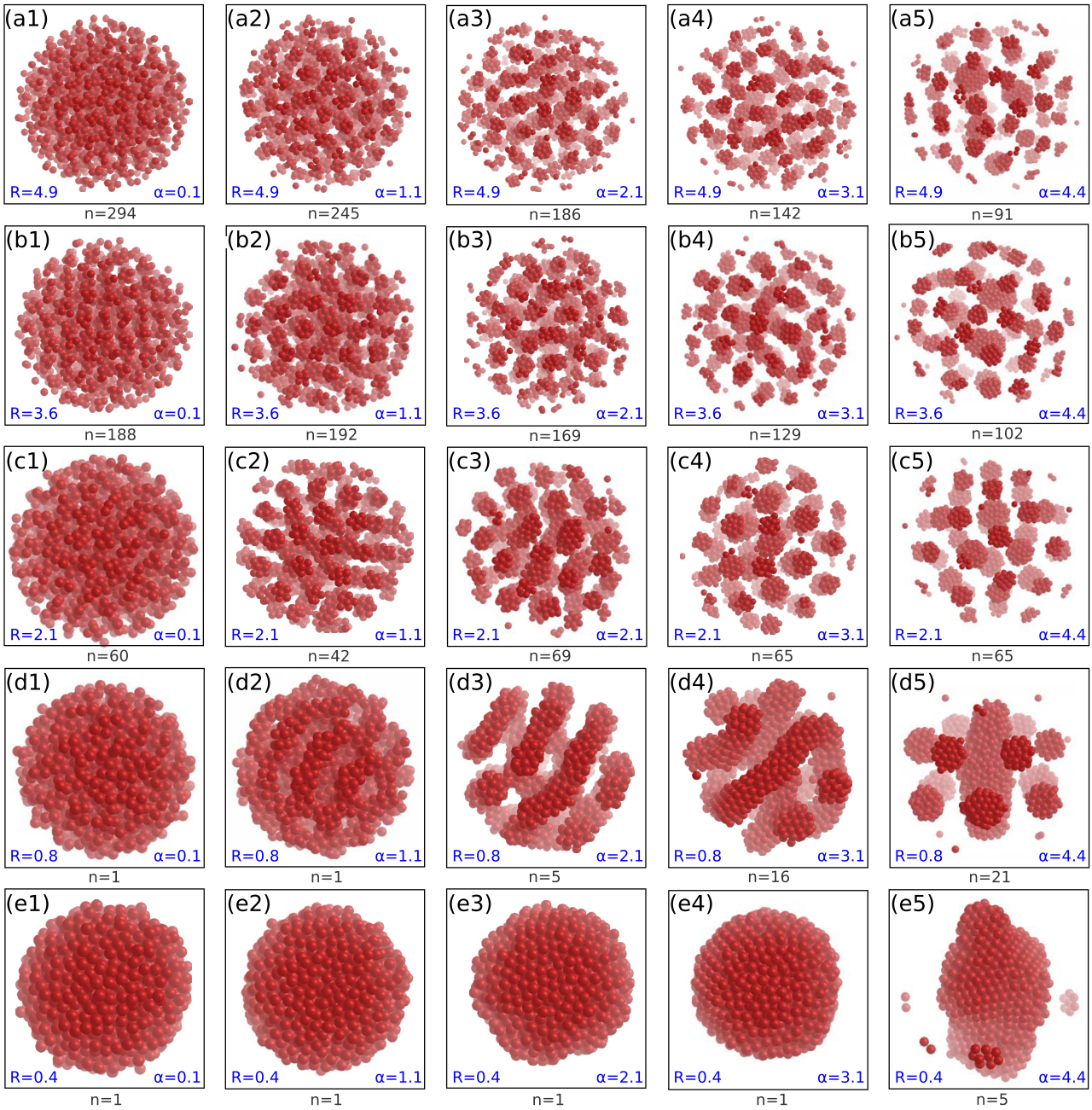

Figure 3. Configurations showing the presence of multiple clusters in the self-assembled structure for some given values of R and α. The values of R and α are fixed at each line and column, respectively. The total number of subclusters, n, is indicated for each case. The labels [(a1)-(e5)] shown within the figure are used to distinguish between different configurations. Each line and column holds, respectively, the same letter and number.

of figure 2(c) have a thickness greater than the particle diameter, and secondly, they are connected by their central regions.

Figure 2(d) shows that the structure is formed by quasi-2D fringed disks. These are formed by more than one layer of particles, are approximately parallel to each other and have no connection through their centers. Note that the quasi-2D fringed disks of figure 2(d) carry the same type of macroscopic arrangement found in 2D clusters, such as those in figure 7(a3) of [47].

The formation of stripes, in 2D systems, was generated by introducing anisotropy in the confinement potential, as shown, for instance, in figure 5(b6) of [51]. In this case, our 3D analogous corresponds to the configuration with rods exhibited in figure 2(e), which was obtained for an isotropic confinement potential.

Figure 3 gives a broad view of the self-assembled configurations for the explored ranges of R and α, and indicates the number n of subclusters for each configuration. We defined that a particle belongs to a given subcluster if it is at a distance $\leqslant 1.1D$ from some other particle belonging to the same subcluster. The internal subclusters are usually bigger than those close to the periphery of the system, as we can see, for instance, in figures 3(b5) and (d5). We can also verify that the increase of R (i.e. of the Gaussian barrier), in general, strongly induces divisions of the system in subclusters. Moreover, the number of particles within a subcluster grows with the value

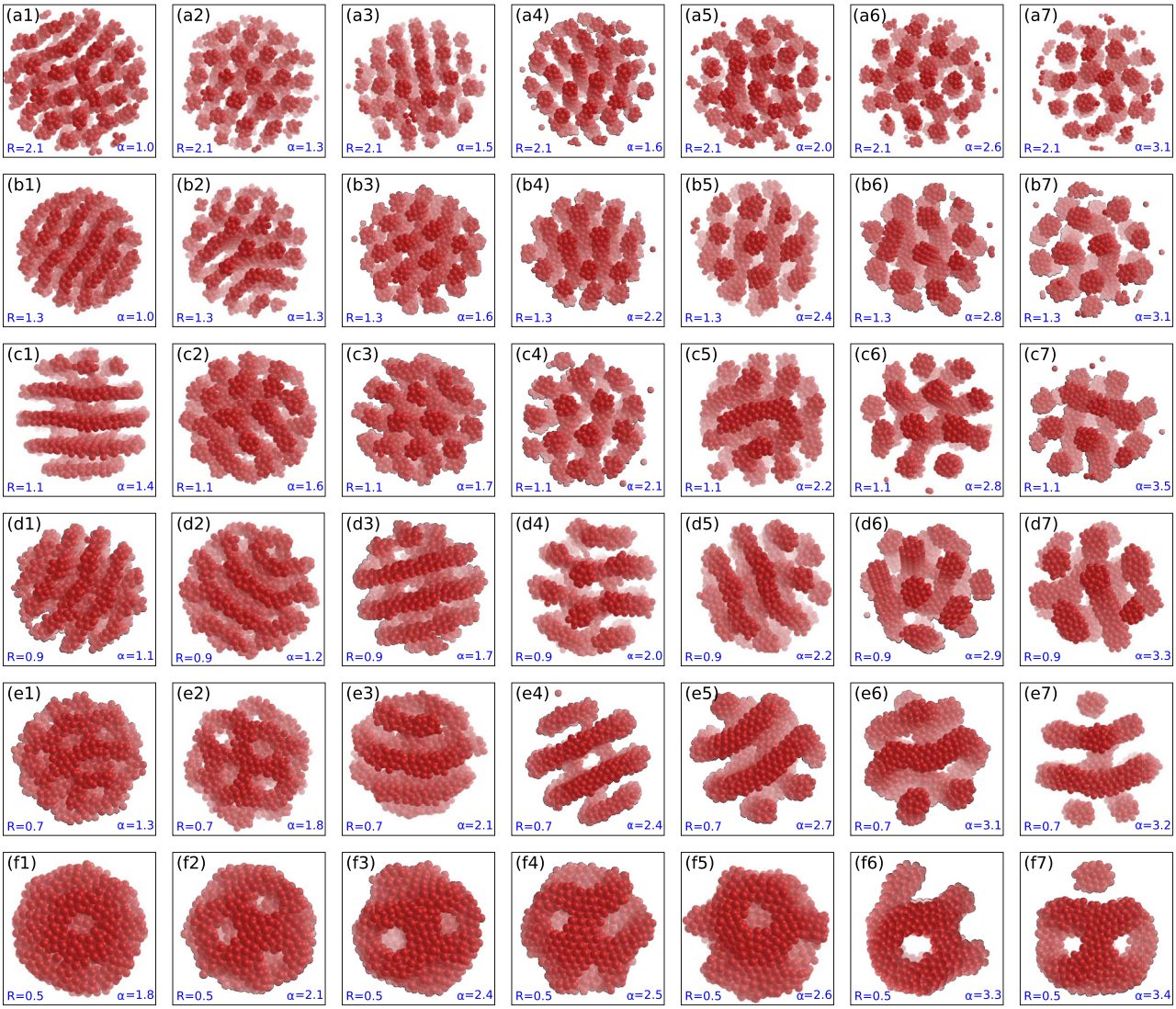

Figure 4. Self-assembled configurations presenting a global ordering for several values of the interaction potential parameters R and α. The configurations were chosen on purpose in order to reveal structural phase transitions. Each line has a fixed value of R while α grows from left to right. The labels [(a1)-(e5)] shown within the figure are used to distinguish between different configurations. Each line and column holds, respectively, the same letter and number.

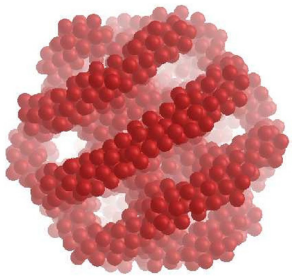

Figure 5. The opposite view of the configuration presented in figure 4(e2). From this point of view we see the precursor of the multiple parallel layer structure.

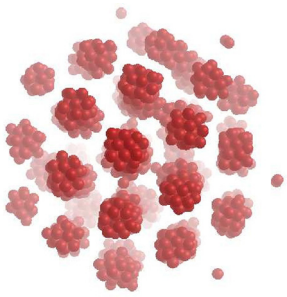

Figure 6. A second viewpoint of the configuration of figure 4(b4), where the axes of the rods are approximatelly perpendicular to the plane of the page. Note that the rods form a hexagonal ordering.

of α, due to the enlargement of the potential well. In addition, the effective resulting potential barrier of the agglomerate also increases. These considerations help us to understand how α can also influence the repulsion between subclusters. For instance, keeping $R = 4.9$, for $\alpha = 0.1$ (see figure 3(a1)) the subclusters are closer than for $\alpha = 4.4$ (see figure 3(a5)).

We observed that, within the ranges $0.5 \leqslant R \leqslant 2.1$ and $1.0 \leqslant \alpha \leqslant 3.5$, a rich variety of structural patterns are formed. We analyzed this region in detail in order to understand the possible structural transitions of the system. This enables us

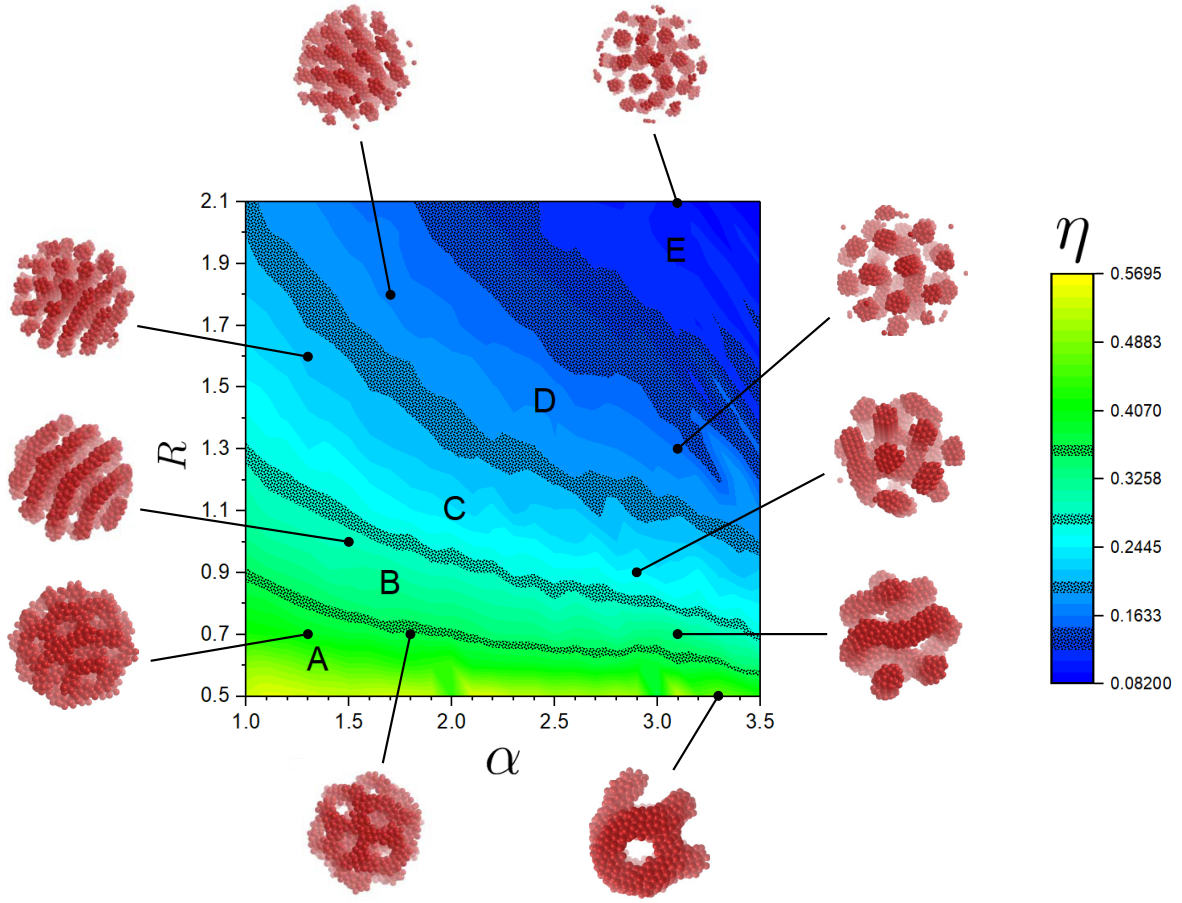

Figure 7. Phase diagram in terms of the packing measure η for $0.5 \leqslant R \leqslant 2.1$ and $1.0 \leqslant \alpha \leqslant 3.5$. Illustrative examples of structures, including all of figure 2, are also displayed. Phase 'A' is characterized by structures with superficial entrances and tunnels, 'B' by disks and circular structures, and 'C' by fringes and fingers. Fragmentation in extended tubes and small subclusters occurs in the structures in 'D' and 'E', respectively.

to understand, for example, how the configurations seen in figure 2 can change and evolve between them.

Figure 4 presents some self-assembled configurations within the mentioned region. The values of R are fixed for each line of the figure, increasing from bottom to top. Whereas α, for each line, increases from left to right. The values of R and α were chosen on purpose in order to highlight the transitions between the macroscopic structures. Because of that, along the same column, the value of α is not kept constant.

The bottom line of figure 4 shows, for increasing α, the following sequence of transitions: spherical shaped structure with superficial entrances (figure 4(f1)), spherical shaped structures with tunnels (figure 4(f3)), open structures (figure 4(f6)) and finally, a structure with two subclusters (figure 4(f7)).

Line (e) in figure 4 makes clear how a spherical tunneled cluster, figure 4(e1), gradually evolves, as α enlarges, to a layered parallel disk configuration connected by their centers, figure 4(e3), a layered parallel disk configuration with a tunneled spherical core, figure 4(e4), a string structure, figure 4(e6) and finally a string structure with clusters, figure 4(e7). Interestingly, figure 4(e5) locally looks similar to a gyroid-like cluster which is one of the stable structures in the bulk [34, 35].

As we have said, the transitions seen in line (e) of figure 4 are gradual. This implies that mixtures of phases can occur which results in configurations with more than one ordering. This fact becomes evident from the configuration for $R = 0.7$ and $\alpha = 1.8$, which holds a mixture of two phases. We show in figure 4(e2) one side of such a configuration, which exhibits a tunneled surface, while the opposite side of the same cluster is shown in figure 5, which presents a structure similar to the parallel layered disks.

For $R = 2.1$, the first line of figure 4 shows the following sequence of global orderings as α increases: a multi-layer fringed disk configuration, figure 4(a1), rods structures, figure 4(a3), and finally, a structure with rounded small subclusters, figure 4(a7). Figures 4(b1) and (a1) have the same value of α, that is, $\alpha = 1.0$, and $R = 1.3$ and $R = 2.1$, respectively. From these two previous configurations we can notice that the increasing of the repulsion leads to the formation of a larger number of layers and fringes. Similarly, the increasing of the repulsion can also lead to the break of the sticks in rounded sub-clusters. This latter transition can be realized when the configurations of figures 4(b7) and (a7) are compared. Also, from the sequence of configurations displayed in figures 4(b2)–(b4), becomes evident that the increasing of α gradually prolongs the fringes up to the formation of sticks or

rods. In order to make the stick configurations clearer we display a second view of figure 4(b4), that is, figure 6. The axes of the rods are approximately perpendicular to the plane of the page and form a hexagonal lattice.

We can see that lines (c) and (d) of figure 4 present the same transitions shown in line (b), and discussed previously. From these three lines, one can presume that the critical values of α, related to the same structural transition, have different magnitudes. For instance, for $R = 0.9$ and $\alpha = 1.7$ (see figure 4(d3)), there is not yet signs of fringes in the disks. On the other hand, for smaller α and larger R, that is, $\alpha = 1.3$ and $R = 1.3$ (see figure 4(b2)) the disks already present fringes. Then, in general, the same transition will occur for smaller α as bigger is R.

Lindquist *et al* [52], using also SALR interactions, found different structures of particles (and voids) depending on the packing fraction, in bulk. In our confined system, we can measure the packing of particles using a procedure similar to the one used in the 2D case of [47, 51]. This is done by evaluating the ratio between $V_p = N\pi D^3/6$ (sum of particles' volumes) and the volume $V_{\rm ch}$ of the convex hull (smallest convex polyhedron that contains all particles). We found that some macroscopic behaviors in figure 4 are correlated to the packing fraction value $\eta = V_p/V_{\rm ch}$.

Figure 7 shows a phase diagram constructed through the simulation results of η for $0.5 \leqslant R \leqslant 2.1$ and $1.0 \leqslant \alpha \leqslant 3.5$, which are the same intervals analyzed in figure 4. In this region, the value of η can indicate several phases found in our system and their transitions. In contrast to the 2D studies, here we can use the packing order parameter, defined on the whole system, to identify a greater variety of patterns. We observed that the intervals $[0.353, 0.366]$, $[0.272, 0.285]$, $[0.19, 0.204]$ and $[0.123, 0.15]$ in η (the dotted regions in figure 7) separate the phase diagram in regions with different structural patterns, that is, regions A, B, C, D and E. As expected for such a complex and finite system, the transitions are not precisely defined.

Examples of structures at some points of the phase diagram are illustrated and indicated in the figure 7, including all cases of figure 2 and some of figure 4. For instance, we have superficial entrances (figure 2(a)) and tunnels (figure 2(b)) in region A. Then disks (figure 2(c)) and circular structures (figure 4(e6)) in region B. As expected, the case of figure 4(e2), which is the same in figure 5, appears in a transition region, that is, between the regions A and B. Fringes (figure 2(d)) and fingers (figure 4(d6)) appear in region C. Finally, in regions D and E we have fragmentation in extended tubes (figures 2(e) and 4(b7)) and in small subclusters (figure 4(a7)), respectively. Note that, the structures found in regions D and E of figure 7 are similar, respectively, to the structures of columns and clusters found in [52] for small packing and without confinement.

4. Conclusions

In conclusion, we have calculated ground state structures for a harmonically confined colloidal system with competing interactions involving a 'mermaid' potential with short-ranged attractions and long-ranged repulsions. We found a wealth of different clusters which can partially be derived and understood by the bulk phases and that in strong 2D confinement. Some of the structures found, however, are very complex and differ in terms of the porosity topology and also in terms of the rim structures. Our results show that many different agglomerate structures can be gained by self-organization of spherical colloids in traps.

Future work should be performed along the following directions. First of all, apart from exploring more parameter combinations of the model proposed here, other 'mermaid-like' pair potentials should be considered to check whether the structures found here are universal or not. This is a challenging task as many different pair potentials are conceivable. Second different kind of confinement should be explored including a hard sphere cavity, a quartic potential or particles within a hard cubic void. Third, a geometry-based theory would be desirable which can in principle predict the structures at least qualitatively. Even if this theory would be purely phenomenological, this would be a formidable achievement. Finally, active systems which are self-propelled represent a flourishing research area [53, 54]. They have been considered recently in the bulk with competing pair interactions [55, 56] and under harmonic confinement [57–62] but not when these two effects are combined. We are expecting complex active molecules [63] with a dynamical function which can emerge on different levels when these active particles possess competing interactions and are confined.

Acknowledgments

HL was supported by the DFG within project LO 418/19-1. We also thanks the Conselho Nacional de Desenvolvimento Científico e Tecnológico (CNPq) for the financial support within project 461296/2014-4.

ORCID iDs

H Löwen https://orcid.org/0000-0001-5376-8062
S W S Apolinario https://orcid.org/0000-0002-5321-741X

References

[1] Lu P J and Weitz D A 2013 *Annu. Rev. Condens. Matter Phys.* **4** 217–33
[2] Deutschländer S *et al* 2013 *Eur. Phys. J. Spec. Top.* **222** 2973–93
[3] Schilling T, Dorosz S, Radu M, Mathew M, Jungblut S and Binder K 2013 *Eur. Phys. J. Spec. Top.* **222** 3039–52
[4] Li B, Zhou D and Han Y 2016 *Nat. Rev. Mater.* **1** 15011
[5] Teixeira P and Tavares J 2017 *Curr. Opin. Colloid Interface Sci.* **30** 16–24
[6] Zhuang Y and Charbonneau P 2016 *J. Phys. Chem.* B **120** 7775–82
[7] Denton A R and Löwen H 1998 *Phys. Rev. Lett.* **81** 469–72
[8] Fischer S, Exner A, Zielske K, Perlich J, Deloudi S, Steurer W, Lindner P and Förster S 2011 *Proc. Natl Acad. Sci.* **108** 1810–4
[9] Bolhuis P, Hagen M and Frenkel D 1994 *Phys. Rev.* E **50** 4880–90

[10] Likos C N, Nemeth Z T and Löwen H 1994 *J. Phys.: Condens. Matter* **6** 10965
[11] Bolhuis P and Frenkel D 1997 *J. Phys.: Condens. Matter* **9** 381
[12] Denton A R and Löwen H 1997 *J. Phys.: Condens. Matter* **9** L1
[13] Malescio G and Pellicane G 2004 *Phys. Rev.* E **70** 021202
[14] Malescio G and Pellicane G 2003 *Nat. Mater.* **2** 97
[15] Norizoe Y and Kawakatsu T 2012 *J. Chem. Phys.* **137** 024904
[16] Batten R D, Huse D A, Stillinger F H and Torquato S 2011 *Soft Matter* **7** 6194–204
[17] Coniglio A, de Candia A and Fierro A 2011 *Mol. Phys.* **109** 2981–7
[18] Spiteri L and Messina R 2017 *Phys. Rev. Lett.* **119** 155501
[19] Archer A J and Wilding N B 2007 *Phys. Rev.* E **76** 031501
[20] Royall C P 2018 *Soft Matter* **14** 4020–8
[21] Stradner A, Sedgwick H, Cardinaux F, Poon W C K, Egelhaaf S U and Schurtenberger P 2004 *Nature* **432** 492
[22] Sear R P and Gelbart W M 1999 *J. Chem. Phys.* **110** 4582–8
[23] Gompper G, Schick M, Domb C and Lebowitz J L 1994 Self-assembling amphiphilic systems *Phase Transitions and Critical Phenomena* (London: Academic)
[24] Orilall M C and Wiesner U 2011 *Chem. Soc. Rev.* **40** 520–35
[25] Mossa S, Sciortino F, Tartaglia P and Zaccarelli E 2004 *Langmuir* **20** 10756–63
[26] Zhang T H, Klok J, Hans Tromp R, Groenewold J and Kegel W K 2012 *Soft Matter* **8** 667–72
[27] Sciortino F, Mossa S, Zaccarelli E and Tartaglia P 2004 *Phys. Rev. Lett.* **93** 055701
[28] Sweatman M B, Fartaria R and Lue L 2014 *J. Chem. Phys.* **140** 03B626
[29] Zhang T H, Groenewold J and Kegel W K 2009 *Phys. Chem. Chem. Phys.* **11** 10827–30
[30] Zhuang Y, Zhang K and Charbonneau P 2016 *Phys. Rev. Lett.* **116** 098301
[31] Ciach A 2008 *Phys. Rev.* E **78** 061505
[32] Archer A J, Pini D, Evans R and Reatto L 2007 *J. Chem. Phys.* **126** 014104
[33] Ciach A and Góźdź W T 2010 *Condens. Matter Phys.* **13** 23603
[34] Edelmann M and Roth R 2016 *Phys. Rev.* E **93** 062146
[35] Pini D and Parola A 2017 *Soft Matter* **13** 9259–72
[36] Ivlev A, Löwen H, Morfill G and Royall C P 2012 *Complex Plasmas and Colloidal Dispersions: Particle-Resolved Studies of Classical Liquids and Solids* vol 5 (Singapore: World Scientific)
[37] Takatori S C, De Dier R, Vermant J and Brady J F 2016 *Nat. Commun.* **7** 10694
[38] Arp O, Block D, Piel A and Melzer A 2004 *Phys. Rev. Lett.* **93** 165004
[39] Arp O, Block D, Klindworth M and Piel A 2005 *Phys. Plasmas* **12** 122102
[40] Bonitz M, Block D, Arp O, Golubnychiy V, Baumgartner H, Ludwig P, Piel A and Filinov A 2006 *Phys. Rev. Lett.* **96** 075001
[41] Bonitz M, Henning C and Block D 2010 *Rep. Prog. Phys.* **73** 066501
[42] Peeters F M, Schweigert V A and Bedanov V M 1995 *Physica* B **212** 237–44
[43] Apolinario S W S, Partoens B and Peeters F M 2006 *Phys. Rev.* E **74** 031107
[44] Bubeck R, Bechinger C, Neser S and Leiderer P 1999 *Phys. Rev. Lett.* **82** 3364–7
[45] Straube A V, Louis A A, Baumgartl J, Bechinger C and Dullens R P A 2011 *Europhys. Lett.* **94** 48008
[46] Liu Y H, Chew L Y and Yu M Y 2008 *Phys. Rev.* E **78** 066405
[47] Costa Campos L Q, Apolinario S W S and Löwen H 2013 *Phys. Rev.* E **88** 042313
[48] McDermott D, Reichhardt C J O and Reichhardt C 2014 *Soft Matter* **10** 6332–8
[49] Almarza N, Pekalski J and Ciach A 2016 *Soft Matter* **12** 7551–63
[50] Greiser C, Ebert S and Goedel W A 2008 *Langmuir* **24** 617–20
[51] Campos L Q C and Apolinario S W S 2015 *Phys. Rev.* E **91** 012305
[52] Lindquist B A, Jadrich R B and Truskett T M 2016 *Soft Matter* **12** 2663–7
[53] Elgeti J, Winkler R G and Gompper G 2015 *Rep. Prog. Phys.* **78** 056601
[54] Bechinger C, Di Leonardo R, Löwen H, Reichhardt C, Volpe G and Volpe G 2016 *Rev. Mod. Phys.* **88** 045006
[55] Mani E and Löwen H 2015 *Phys. Rev.* E **92** 032301
[56] Rein M and Speck T 2016 *Eur. Phys. J.* E **39** 84
[57] ten Hagen B, van Teeffelen S and Löwen H 2011 *J. Phys.: Condens. Matter* **23** 194119
[58] Pototsky A and Stark H 2012 *Europhys. Lett.* **98** 50004
[59] Volpe G and Volpe G 2013 *Am. J. Phys.* **81** 224–30
[60] Szamel G 2014 *Phys. Rev.* E **90** 012111
[61] Nourhani A, Crespi V H and Lammert P E 2015 *Phys. Rev. Lett.* **115** 118101
[62] Ribeiro H and Potiguar F 2016 *Physica* A **462** 1294–300
[63] Löwen H 2018 *Europhys. Lett.* **121** 58001